THE JOURNAL OF PHYSICAL CHEMISTRY C

pubs.acs.org/JPCC Article

Spectroscopic Signatures of the B and H_4 Polyatomic Nitrogen Aggregates in Nanodiamond

Ryan A. Beck, Lixin Lu, Alessio Petrone, Amanda C. Ong, Peter J. Pauzauskie, and Xiaosong Li*

Cite This: *J. Phys. Chem. C* 2020, 124, 18275−18283 Read Online

ACCESS | Metrics & More | Article Recommendations | Supporting Information

ABSTRACT: Defects within nanodiamonds have enabled a variety of quantum sensors based on optical properties that are sensitive to pressure, optical/electric fields, and the configuration of both electronic and nuclear of spins. The presence of dopants can introduce midgap states influencing their optical properties. Complex defects based on nitrogen aggregates have been shown to form in nitrogen-containing diamonds; as such, it is important to differentiate these systems from pure diamond and single nitrogen vacancy (NV) systems. Here we report the effect of N_4V_x B- and H_4-aggregate defects on the infrared vibrational, optical, and X-ray absorption spectroscopies of nanodiamonds. It is found that the presence of these polyatomic nitrogen-aggregate defects introduces unique vibrational responses, as well as electronic levels giving rise to unique optical and X-ray absorption features.

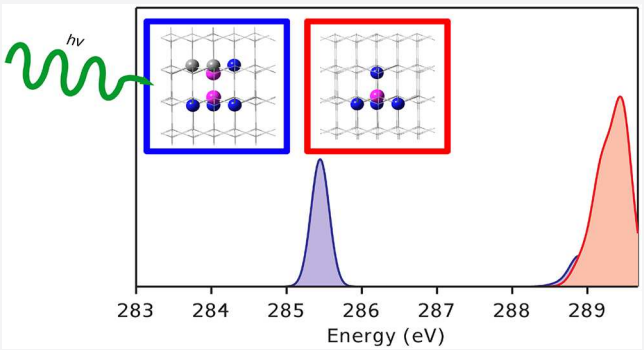

INTRODUCTION

Nanodiamonds have promise for use in applications ranging from bioimaging to spin qubits.[1−13] While pure diamond gives rise to a large bulk optical band gap (~5.5 eV),[14] the addition of defects can be used to introduce discrete electronic levels within the gap. By controlling the size of the nanodiamond to the nanoregime (~5 nm in diameter) quantum confinement effects widen the band gap, and as such enable the tunability of the transitions.[2,15,16] This combined with the rigidity of the diamond lattice which inhibits defect diffusion and phase transitions at high temperatures and pressures make diamond a compelling material for study.[5,8,13] Nitrogen is a ubiquitous impurity in natural and synthetic nanodiamonds as it is difficult to fully isolate the systems from the environment. Single nitrogen-vacancy (NV) centers have been reported to have either a reduced-triplet or a neutral-doublet ground state, with the triplet state being the more stable ground-state configuration.[10,17−20] The electronic structures, quantum confinement, and spectroscopic signatures of single NV centers have been thoroughly investigated previously,[10,17−23] with the diamonds containing these NV centers labeled as type Ia diamonds. Depending on the structure and arrangement of the nitrogen atoms in the diamonds, as well as the conditions where the diamonds were formed, aggregate systems, known as either "A" centers or "B" centers, can form, classifying the diamonds as type IaB.[24] These aggregate systems are classified by the number of nitrogens and vacancies contained within the defect. While significant work has gone into studying the A centers within diamonds,[25−27] less has been done for the B centers, the dominant form in type IaB diamonds.[24,28] The form of the B center consists of four nitrogen atoms surrounding a single vacancy,[24] and more work is needed to identify the spectroscopic signatures of these B-center systems. The nitrogen-aggregates of central interest in this study are the N_4V (B-aggregate)- and N_4V_2 (H_4-aggregate)-doped systems as named in ref 29. They are identified theoretically through the complete neglect of differential overlap (CNDO) molecular-orbital *semiempirical* method[30] to be the more stable of the aggregate configurations. These aggregate systems typically first exist as A aggregates (pairs of nitrogen atoms) where then, with enough time and pressure, two A centers can trap a vacancy forming the B-aggregate, the structure of which is shown in Figure 1, consisting of four nitrogen atoms surrounding a vacancy. If the B-aggregate acquires an additional vacancy and is able to undergo a slight structural rearrangement, the H_4-aggregate system is formed (Figure 1).[29] The presence of these dopants can affect the selection rules for both the vibrational Raman and infrared absorption spectra, as well as introduce midgap states that give rise to unique UV−visible (vis) as well as X-ray absorption spectral features. In addition, nanodiamonds have a pre-edge feature in the carbon K-edge energy region which has been suspected of

Received: April 7, 2020
Revised: July 21, 2020
Published: July 21, 2020

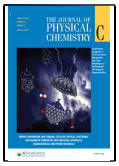

https://dx.doi.org/10.1021/acs.jpcc.0c03106
J. Phys. Chem. C 2020, 124, 18275−18283

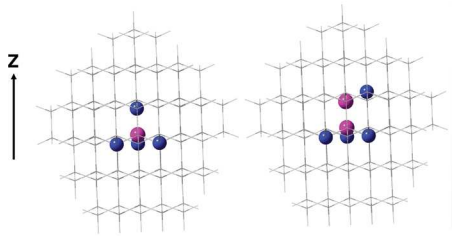

Figure 1. Doped 1.2 nm $C_{116}N_4H_{104}$ (as B aggregate, left) and $C_{115}N_4H_{104}$ (H_4 aggregate, right) ball and stick representations of the replaced atoms in the pure diamond matrix (this last represented as wireframe), nitrogen in blue and vacancy(s) in pink. The labeled *Z* axis is along the crystallographic ⟨1, 1, 1⟩ axis.

arising from either sp^2 carbon arising from surface rearrangement[12] or as a result of the presence of midgap states arising from the presence of dopants.[11]

In this work, we carry out a systematic spectroscopic study using density functional theory (DFT) and time-dependent DFT (TDDFT) combined with a cluster approach for modeling the nanodiamonds. DFT/TDDFT, combined with the cluster approach, has been able to provide needed insight for the characterization of excited states in doped semiconductor quantum dots and molecules,[23,31,32] as well as shed insight into the vibrational properties of molecules and semiconductor quantum dot systems.[11−13,33] This work focuses on the effect of the presence of the N_4V_x-aggregates on the vibrational, UV/vis, and X-ray spectral properties of nanodiamond systems.

METHODOLOGY

Nanodiamonds were constructed to be nearly spherical with a bulk fcc lattice parameter of a = 0.357 nm[14] according to the procedure presented in ref 10. Hydrogen atoms were used to passivate the surface carbon dangling bonds. Although other moieties are generally present on the surface, chemical treatments of the surface can provide a more uniform passivation.[2,34,35] A $C_{121}H_{104}$ (diameter ∼ 1.2 nm) cluster was used as the starting model for the nitrogen-aggregate-doped systems previously shown to be of an appropriate size to accurately capture optical and vibrational transitions due to the presence of both defects and surface reorganization.[11−13] Figure 1 shows the structures of the as-prepared aggregate-containing nanodiamond systems.

The N_4V center was created by replacing five carbon atoms near the center of the pure nanodiamond constructed from bulk parameters along the ⟨1, 1, 1⟩ axis of the model with four nitrogen atoms and positioning the vacancy at the center, assuming the so-called B aggregate configuration (Figure 1). This defect has a local symmetry of T_d within the C_{3v} diamond host lattice. The N_4V_2-doped system was obtained by further replacing a carbon atom along the ⟨1, 1, 1⟩ axis with a vacancy and replacing one of the neighboring carbons with a nitrogen resulting in a C_s symmetry. The pure diamond, B-aggregate, and H_4-aggregate systems were then independently fully optimized, and harmonic vibrational analysis was performed to verify the obtained geometries were true minima. Geometries were considered optimized when both the forces [maximum and root-mean-square (rms) of the force 0.000450 and 0.000300 hartree/bohr, respectively] and displacement [maximum and rms displacement 0.00018 and 0.0012 bohr, respectively] values were below the threshold criteria. The systems are similar to, but slightly smaller than, commercially available nanodiamonds from laser-heated diamond anvil cell or detonation synthesis.[2,36,37] Although the size of the systems in this study might show enhanced quantum confinement effects with respect to the commercially available systems, the interplay between optical signatures due to the presence of the defects and the nano size are well represented and can be used to provide theoretical grounds for understanding larger, though still quantum confined, systems. Given that the Bohr exciton radius for diamond is ∼1.6 nm,[38] the electronic properties of these diamond clusters are expected to exhibit quantum confinement effects.[10]

Calculations were preformed using the Gaussian[39] electronic structure software package. The ground-state electronic structures were obtained by solving the Kohn−Sham equation using the hybrid Becke, three-parameter, Lee−Yang−Parr functional with the Coulomb-attenuating approach (CAM-B3LYP)[40−43] with a 6-31++G(d,2p) basis. A basis set with a large spatial extent (i.e., diffuse funtions) has been utilized as it has been previously demonstrated to be important for describing low-energy Rydberg-like states created by C−H bonds (in this case the surface of the nanodiamonds).[44,45] These states may also play an important role for shallow-implanted centers in diamond.[45] On the other hand diffuse functions have been previously shown to be less important for localized defects located far from the surface.[46−48] Given the sensitivity of CAM-B3LYP to the treatment of exact exchange, it is able to outperform other canonical hybrid (i.e., B3LYP, PBE0, and so on) functionals for the description of the Rydberg-like and charge-transfer states.[49−51] Because these Rydberg-like states may influence the defect energy levels within the diamonds and the quantum confinement effect of these dots,[11] CAM-B3LYP/6-31++G(d,2p) was used for this investigation. The electronic structures of excited states were calculated using time-dependent density functional theory within the linear response framework (LR-TDDFT)[49,51,52] and its energy specific implementation for computing X-ray near-edge absorption spectra (XANES).[53,54] Given that XANES spectra probe the transitions from atomic 1s to valence transitions, the energy range for the energy window in ES-TDDFT was selected as the difference between the carbon or nitrogen, respectively, 1s orbital(s) and the lowest unoccupied orbitals with an additional ∼10 eV shift to ensure that all roots were accounted for (∼250 eV and ∼350 eV for carbon and nitrogen, respectively).

RESULTS AND DISCUSSION

Charge and Spin States. The charge and multiplicity for the B- and H_4-aggregate systems have not been well studied previously. As a result, several different possibilities for both defect structures were tested herein. A range of charges and multiplicities of the aggregate systems were examined by comparing their formation energies (eq 1) and the difference between their highest occupied molecular orbital (HOMO) and lowest unoccupied molecular orbital (LUMO). The results are tabulated in Table 1.

Given that the defects have different numbers of electrons among the various spin states, their total energies cannot be directly compared. Thus, the formation energy of a point defect in the nanodiamond was calculated using eq 1.

$$\Delta E_{\text{defect}}(q) = E_{\text{supercell}} - E_{\text{pure}} + \Sigma_i n_i \mu_i + \mu_e \quad (1)$$

https://dx.doi.org/10.1021/acs.jpcc.0c03106
J. Phys. Chem. C 2020, 124, 18275−18283

Table 1. LUMO−HOMO Energy Difference, $\Delta\epsilon$ in eV, for the Examined Potential Electronic States (Charge and Multiplicity) for the H_4- and B-Aggregate-Doped 1.2 nm Nanodiamond Systems Optimized at the CAM-B3LYP/6-31++G(d,2p) Level of theory[a]

		B-aggregate		H_4-aggregate	
charge	multiplicity	$\Delta\epsilon$ (eV)	ΔE_{defect} (eV)	$\Delta\epsilon$ (eV)	ΔE_{defect} (eV)
−2	triplet	1.11	8.34	1.05	10.82
−2	singlet	0.81	8.71	0.77	11.90
−1	doublet	0.87	4.79	2.56	6.95
0	triplet	1.08	12.96	5.23	11.97
0	singlet	5.79	3.69	5.60	7.00
1	doublet	3.84	15.53	5.40	17.84
2	triplet	0.04	32.61	3.68	34.74
2	singlet	2.39	34.00	2.94	34.63

[a]At this level of theory, the ∼1.2 nm diameter pure diamond has a LUMO−HOMO difference of 7.17 eV.

where $E_{supercell}$ and E_{pure} are the total energies for the defect-containing and pure systems, respectively. Equation 1 accounts for the removal and addition of different atoms in the system (represented as the chemical potentials, felt by the chemical system, introduced by atoms removed from or added to the system, $+\mu$ or $-\mu$) as well as the difference between the charge of the systems, q, and the effect of the charge on the host crystal given by the μ_e term. Chemical potentials used for the calculation of formation energy were taken from DFT results, detailed in the Supporting Information.

The experimentally determined zero-phonon line for bulk diamonds containing B-aggregates has been previously identified at 5.26 eV, which is comparable with the neutral-singlet LUMO−HOMO difference of 5.79 eV,[24] suggesting that the neutral singlet is the most likely state. It is important to note that these band gaps are only examined through the difference between HOMO and LUMO, and the optical features may be of a slightly lower energy in the linear-response TDDFT framework when the electron−hole interaction is considered. In addition, this neutral, singlet state is associated with the lowest formation energy indicating that the neutral-singlet B-aggregate is most likely to form.

In the case of the H_4-aggregate system, the experimentally measured photoluminescent (PL) feature for the H_4 defect is 2.50 eV.[26] There are several states (the negative doublet, neutral singlet and triplet, and the positive triplet and singlet) that have the HOMO/LUMO gap close to this energy. Through examination of the formation energies for the H_4-aggregate, the negative-doublet and the neutral-singlet states of the H_4 defect are most likely to form. Optical spectra (see Figure S1 in the Supporting Information) computed using linear-response TDDFT show that the first excitation for the negative doublet lies at 1.33 eV and the neutral-singlet state has the first feature at 3.35 eV. As such the neutral-singlet state was chosen for further investigation, noting that the quantum confinement effect will influence the absorption spectra for these systems, causing them to be higher than experiment.

Structures of B- and H_4-Aggregates. As shown in Figure 1, the initial structure for the B-aggregate system has a local tetrahedral T_d symmetry in the C_{3v} diamond lattice. The H_4-aggregate system, however, with its additional vacancy, does not have a tetrahedral symmetry; instead it has an initial symmetry of C_s. Figure 2 shows the local effects of the geometry relaxation on the defects after the systems were fully optimized.

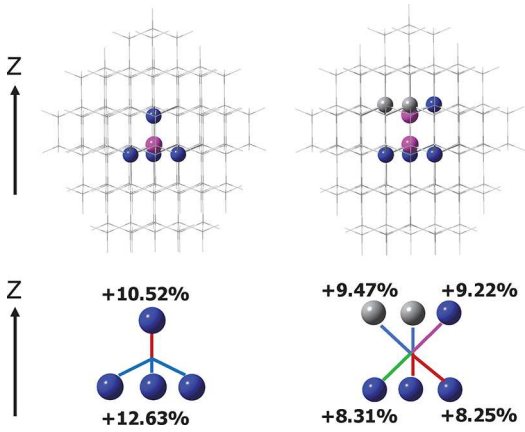

Figure 2. Geometry relaxation near the B- and H_4-aggregate centers ($C_{116}N_4H_{104}$ and $C_{115}N_4H_{104}$, respectively) for the 1.2 nm diameter nanodiamonds. Systems were optimized at the CAM-B3LYP/6-31++G(d,2p) level of theory. Left is the B-aggregate system with right being the H_4-aggregate system; top is the defect (nitrogen in blue, vacancies in pink) with the rest of the diamond in wireframe; bottom shows the expansion, in percent, from the original, crystallographic bond length of 1.5446 Å, with similar colors corresponding to equal expansions.

Upon optimization, the aggregate-containing systems expand out from the vacancies, compared to the initial diamond-like structures. In the case of the B-aggregate, a pseudotetrahedral local symmetry is mostly preserved with the NV bond length increased by 10.5%−12.6% compared to the crystallographic bulk diamond bond length of 1.5446 Å. The slight symmetry breaking is due to the C_{3v} symmetry of the host nanodiamond. In the case of the H_4-aggregate system, in addition to the increased NV bond lengths, nearest carbon-vacancy bonds also increase by ∼9%. This increase in bond length has been noted before arising from the increased charge density in the vacancy given by the nitrogen atoms.[29]

Vibrational Analysis. Structural analysis suggests that vibrational spectroscopy can be used to differentiate between the different aggregates. While the Raman spectra are known to lack unique features that can be used to probe the nature of the nitrogen aggregate defect (see Figure 3 for the pure diamond and B-aggregate Raman comparison),[28] the infrared (IR) spectra for the aggregate systems show several spectroscopic features different from both the pure nanodiamonds and the nitrogen-vacancy-containing nanodiamonds.

Plotted in Figure 4 are the calculated IR spectra for the pure diamond, nitrogen-aggregates, and NV^- systems. It can be noted that each species contains the diamond band at ∼1330 cm^{-1}.[55−57] Please see ref 12 for a more detailed examination of the pure diamond cluster vibrational properties. The area with the largest, most notable, differences between the aggregate and nonaggregated systems occurs in the ∼800 to ∼1200 cm^{-1} range. Given that this region has significant overlap from surface hydrogen−carbon−hydrogen bending modes, in an effort to isolate the responses due to the carbon and nitrogen vibrations, the mass of the surface hydrogen was artificially increased for analysis as has been reported in various studies examining nanodiamond vibrational spectroscopy.[11,12,58,59] As can be seen in Raman spectra (Figure 3), in the case of both

https://dx.doi.org/10.1021/acs.jpcc.0c03106
J. Phys. Chem. C 2020, 124, 18275−18283

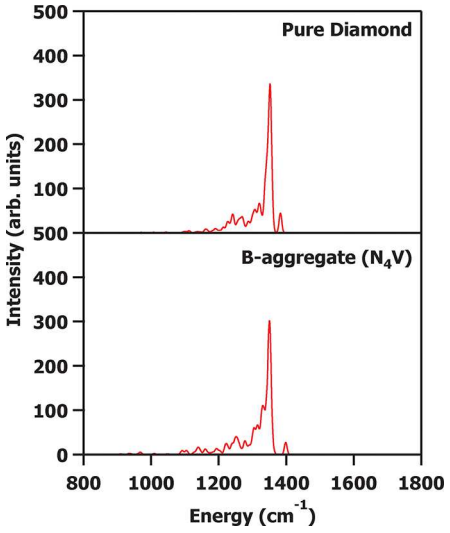

Figure 3. CAM-B3LYP/6-31++G(d,2p) Raman spectra for the pure ∼1.2 nm diamond (top) and the N_4V-doped "B-aggregate" diamond (bottom) with artificially heavy hydrogen mass. As can be noted, the pure diamond peak at ∼1300 cm^{-1} is prominent, and there are not significant differences between the spectrum with and without the nitrogen aggregate.

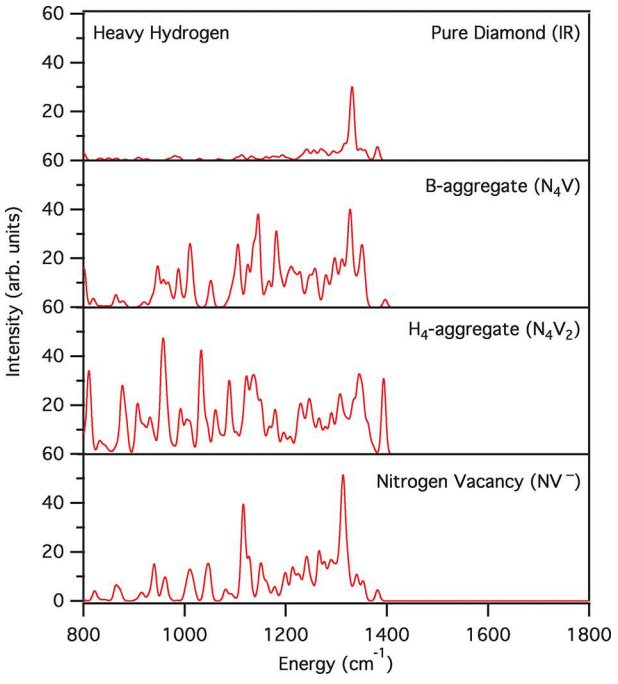

Figure 4. CAM-B3LYP/6-31++G(d,2p) IR spectra for, in descending order, the ∼1.2 nm diameter pure diamond, B-aggregate containing diamond, the H_4-aggregate containing diamond, and the NV^- diamond with artificially large hydrogen mass. The IR spectra with regularly massed hydrogen can be located in the Supporting Information (Figure S4). IR activity has a 4 cm^{-1} broadening applied to generate the spectra for all four plots.

the pure and NV^--doped nanodiamonds the region of ∼800−1200 cm^{-1} is mostly featureless. The addition of nitrogen-aggregate systems slightly increases the IR activity in this spectral region, and gives rise to one strong feature at 1116 cm^{-1}, corresponding to an *E* vibration comprising mostly the carbon lattice of the diamond (see Figure S2 in the Supporting Information).

Examining the IR spectra in Figure 4, we identify that both of the aggregate systems contain increased responses in the ∼1095 cm^{-1} energy region, when compared to both the pure and NV^- systems. In the case of the B-aggregate system, this vibration corresponds to an A_1 vibration primarily involving the diamond lattice around the nitrogen defect. For the H_4 defect, this is an A′ vibration which involves both the diamond lattice as well as the nitrogen aggregate. Both of these vibrations have their displacement vectors displayed in Figure S3.

While IR spectroscopy is able to differentiate the nitrogen aggregate systems from both pure diamond and NV^--doped diamonds with a fine enough resolution, the spectra for both of the aggregate systems is very similar given their similar geometries. There are two regions that show significant IR activities between the H_4- and the B-aggregate systems. At 1009 cm^{-1} which corresponds to an A_1 vibration, plotted in Figure S5, the B-aggregate system, compared to the H_4-aggregate, shows an increased IR activity. The 1009 cm^{-1} vibration comprises mostly the diamond lattice around the aggregate center similar to the ∼1095 cm^{-1} vibration. On the other hand, responses with an increase in activity for the H_4-aggregate system, compared to the B-aggregate, can be seen at 942 and 1035 cm^{-1}. The 942 cm^{-1} vibration has A′ character, and mostly involves the "top" (as shown in Figure 1) nitrogen and vacancy within the diamond lattice. The 1035 cm^{-1} vibration has A″ character and mostly involves the "bottom", as defined in Figure 1, three nitrogens and vacancy. Both of the vibrations are plotted in Figures S6 and S7. These features can be difficult to experimentally resolve; however, recent work has been realized in aberration corrected, energy filtered low-loss electron energy loss spectroscopy enabling resolution reaching 5 meV which has allowed for the measurement of isotopically labeled bonds in molecular crystals.[60] These developments in combination with the photothermal heterodyne spectroscopic techniques may enable the experimental measurement of point defects in individual nanodiamonds.[61] As such the ab initio insights provided are important for distinguishing these nitrogen-containing systems. To be able to further separate the two aggregate systems, the electronic structures have been investigated.

Ground State Electronic Structures. The electronic density-of-states (DOS) plots in Figure 5 show the presence of defect-centered intraband states when the defects are present in comparison to the pure diamond. The frontier molecular orbitals for the B- and H_4-defects are represented in Figure 6, which appear as intraband states. In the case of the B-aggregate system, given that the overall symmetry of the diamond has relaxed from tetrahedral to C_{3v}, the tetrahedral t_2 orbitals are split into e and a_1 orbitals, shown in Figure 6. It is interesting to note that the a_1 orbital of the B-aggregate is higher in energy than e_x and e_y orbitals unlike what is seen for the NV^- system.[10]

The presence of the H_4-aggregate causes the e_x and e_y orbitals to further split into the a′ orbitals that can be seen in Figure 6. These orbitals remain localized around the bottom (Figure 1) nitrogen atoms and vacancy with a large nitrogen contribution. The HOMO level for the H_4-aggregate system is localized on the top nitrogen and vacancy with a significant carbon contribution. Not only does the N_4-aggregate introduce the intraband occupied orbitals it also contributes to the unoccupied levels which lie near the valence band edge. The difference in localization for these systems can be viewed in the

https://dx.doi.org/10.1021/acs.jpcc.0c03106
J. Phys. Chem. C 2020, 124, 18275−18283

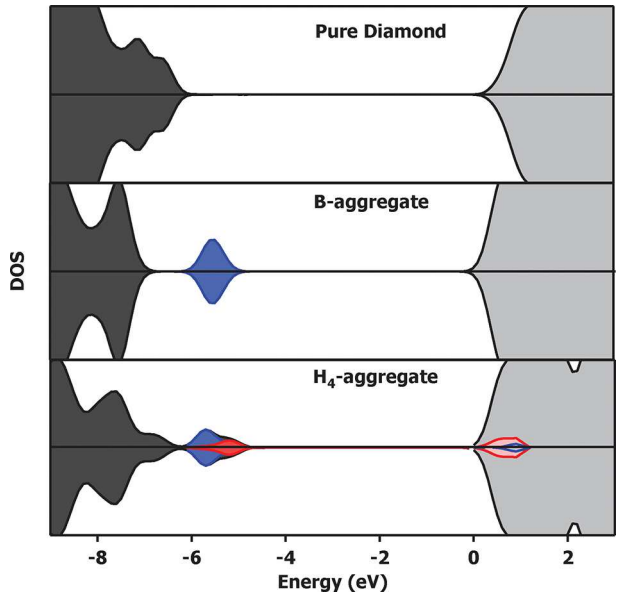

Figure 5. Density of states plots for the pure diamond (top), B-aggregate (middle), and H_4-aggregate (bottom) neutral, singlet systems identified earlier to be most probable. Contributions to the intraband states due to the defect are shown with nitrogen contributions in blue and, in the case of the H_4-aggregate, the carbons surrounding the "top" vacancy in red. The partial DOS contributions by both carbon and nitrogen have been multiplied by a factor of 2. The occupied orbitals are shown with a darker plot against the unoccupied orbitals.

Supporting Information (Figures S8 and S10). The significantly different localization schemes and symmetries of the intraband molecular orbitals localized around the B- and H_4-aggregate defects suggest that the two systems will have unique and distinct features in UV/vis spectra.

UV/Vis Spectra. The optical response of the nanodiamond systems in the UV/vis region has been examined using the linear response TDDFT formalism. Table 2 lists the first four excitations for both aggregate systems, and the simulated absorbance spectra can be viewed in Figure 7. For the size of nanodiamond studied here, the band-to-band excitation (not shown) appears at ~7 eV. The spectral features in Figure 7 arise from transitions between defect levels to the conduction band edge of the nanodiamond. These transitions are red-shifted from the pure diamond band−band transitions as they originate from the orbitals introduced into the midgap by the

Table 2. CAM-B3LYP/6-31++G(d,2p) Linear Response TDDFT Results for the Diamond Systems[a]

species	absorption (eV)	oscillation strength	contributing molecular orbitals
B-aggregate	4.47	0.0048	HOMO → LUMO
	4.52	0.0581	HOMO(−1) → LUMO
	4.52	0.0581	HOMO(−2) → LUMO
	4.60	0.0064	HOMO → LUMO(+1)
species	absorption (eV)	oscillation strength	transition character
H_4-aggregate	3.35	0.0020	a′ (HOMO) → a″
	3.52	0.0316	a′ (HOMO) → a″
	4.15	0.0010	a′ (HOMO-2) → a″
	4.16	0.0144	a′ (HOMO-2) → a″

[a]The corresponding orbitals are plotted within Figure 6.

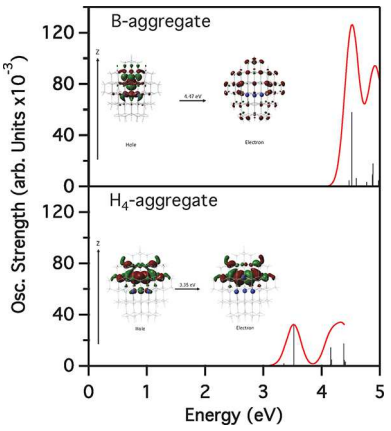

Figure 7. UV/vis spectra for the B-aggregate system (top panel) and the H_4 aggregate system (bottom panel) at the LR-TDDFT CAM-B3LYP/6-31++G(d,2p) level of theory. A Gaussian broadening term has been applied to the transitions (represented as black sticks) of 0.12 eV. Inset are the natural transition orbitals (NTOs)[62] for the hole (left) and electron (right) orbitals for the first transition in B-aggregate and H_4-aggregate, respectively.

aggregate as shown in Figure 6. The absorption spectra of the B- and H_4-aggregates differ significantly from that of the NV^--containing nanodiamond, which has features starting at ~2 eV enabling the differentiation between aggregate systems and nitrogen vacancies.[10]

The first absorption response occurring at ~4.5 eV for the B-aggregate is significantly red-shifted when compared to the

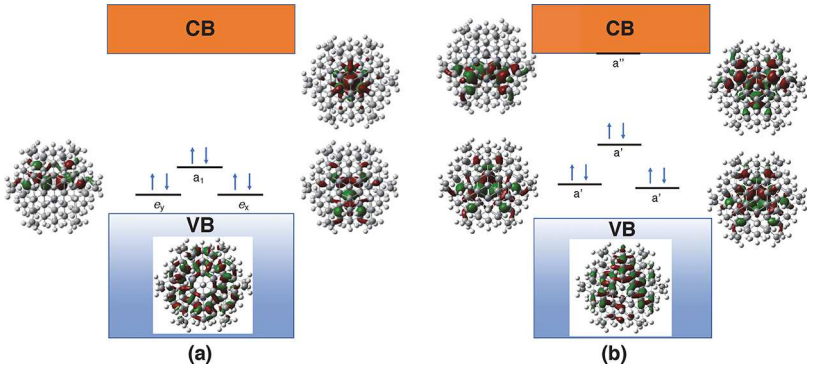

Figure 6. Molecular orbital diagrams for the neutral singlet, (a) B-aggregate and (b) H_4-aggregate systems. Inset pictures are plots of the MOs corresponding to the energy levels. Each surface has an isovalue of 0.03. The positioning of the MO levels is not drawn to scale.

https://dx.doi.org/10.1021/acs.jpcc.0c03106
J. Phys. Chem. C 2020, 124, 18275−18283

literature absorption of ∼5.3 eV.[24] This can be attributed to the formation of Rydberg-like unoccupied states, which are visualized in Figure S9 for the ∼1.2 nm nanodimaond. These states have been observed previously with hydrogen-capped ultrasmall diamond nanoparticles (adamantane, diamantane, and so on) as the cause of experimental band gaps lower than anticipated, which were able to be described through TDDFT.[44] It can be seen in Figure 7 and Table 2 that there are two degenerate responses with significant intensity corresponding to transitions from the e_x and e_y MOs, respectively, to the LUMO. As can be noted from the insets in Figure 6, these orbitals have a larger spatial extent through the diamond than the a_1 orbital. As a result, transitions from e_x and e_y MOs are associated with a greater overlap with the conduction band orbital and thus a significantly larger intensity in the absorption spectrum.

The H_4-aggregate has several absorption features which appear red-shifted compared to those in the B-aggregate, as the H_4-aggregate system introduces localized states both at the valence band edge and conduction band edge (Figure 6). The lowest energy spectral peak at ∼3 eV consists of defect-centered transitions mixed with conduction band characters. This initial transition consisting of the a′ to a″ orbitals (Table 2) is significantly red-shifted when compared to the B-aggregate spectrum. Since the first transition for the H_4-aggregate center is defect-centered, the red-shift from the presence of the Rydberg states is less than for the B-aggregate.[11] While the B-aggregate excitation is largely size invariant, the spectral features of H_4-aggregate shows clear signs of quantum confinement. As previously noted,[29] and can be visualized in the inset of Figure 7, the electron and hole properties of the H_4-aggregate are localized to the top nitrogen and vacancy, but more delocalized compared to that of B-aggregate. As a result, UV/vis spectral features of H_4-aggregate are more sensitive to the quantum confinement.

X-ray Absorption. XAS is sensitive to elemental composition of the material being probed as well as changes to the structure of the material. The XAS K-edge feature specifically examines the transition from 1s core electrons to virtual valence molecular orbitals. XAS thus can be used to study local properties of the absorbing centers. In nanodiamonds there has been previous success in characterizing heteroatomic dopants and in the study of surface reconstruction using carbon K-edge spectral features.[11,12,63−68] As has been both experimentally and theoretically identified, the surface reconstruction of the nanodiamonds causes a pre-edge feature to appear in the carbon K-edge energy region of the XAS, commonly attributed to the carbon 1s to carbon π^* orbitals lying on the surface of the diamond.[12,36,67] In a recent work it was shown that silicon-vacancy defect was able to introduce similar pre-edge features in nanodiamonds.[11]

In this section, carbon and nitrogen K-edge XAS are examined for nanodiamonds containing different polyatomic nitrogen defect configurations. Figure 8 and Table 3 compare XAS carbon K-edge spectra in several different defect-containing nanondiamond. The pure diamond has one major peak appearing at ∼289 eV corresponding to carbon 1s to σ^* transitions. In the case of the B-aggregate system there is a lack of a noticeable pre-edge feature. As can be determined from Figure 5, the B-aggregate does not introduce unoccupied intraband orbitals. As a result, the carbon K-edge spectrum of the B-aggregate is similar to that of pure diamonds.

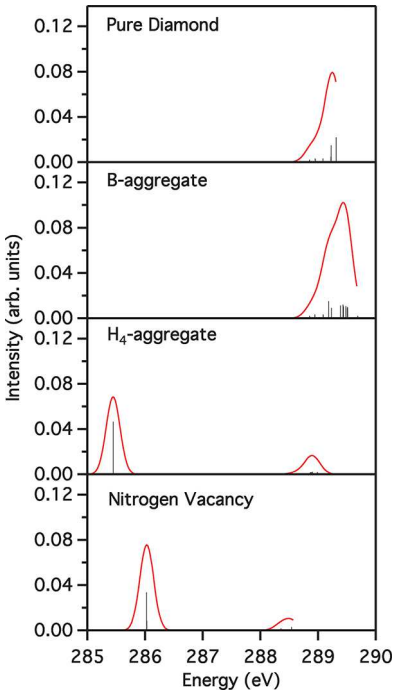

Figure 8. CAM-B3LYP/6-31++G(d,2p) carbon K-edge for the d = ∼1.2 nm nanodiamond systems, uniformly shifted by 13 eV to better align with experimental values. Plotted, in descending order, are the spectra for the pure diamond, the B-aggregate system, the H_4-aggregate system, and the NV^- system. The first (shifted) excitations are listed in Table 3, with the NTOs responsible for the bolded excitations shown in the SI (Figures S12−S18).

Table 3. CAM-B3LYP/6-31++G(d,2p) TDDFT XAS Results for the Carbon and Nitrogen K-Edge[a]

species	ω (eV)[b]	transition characters
pure nanodiamond	**288.85**	carbon 1s → σ^*
	288.95	carbon 1s → σ^*
	289.08	carbon 1s → σ^*
	289.22	carbon 1s → σ^*
B-aggregate	**288.85**	carbon 1s → σ^*
	288.94	carbon 1s → σ^*
	289.09	carbon 1s → σ^*
	289.18	carbon 1s → σ^*
	402.72	nitrogen 1s→ σ^*
	402.84	nitrogen 1s→ σ^*
H_4-aggregate	**285.44**	carbon 1s → a″
	285.45	carbon 1s → a″
	288.57	carbon 1s → a″
	288.65	carbon 1s → a″
	402.10	nitrogen 1s→ a″
	402.10	nitrogen 1s→ a″
	402.15	nitrogen 1s→ a″
NV^-	**286.03**	carbon 1s → e_y
	286.03	carbon 1s → e_x
	286.03	carbon 1s → e_y
	402.06	nitrogen 1s → σ^*

[a]The NTOs for the bolded excitations are plotted in the SI (Figures S12−S15). [b]Please note values are uniformly shifted by 13 eV to better align theoretical results with experimental spectra.[11]

In contrast, unoccupied intraband levels in nanodiamonds containing H_4 and NV^- defects give rise to a noticeable pre-edge feature. This feature corresponds to transitions from the

https://dx.doi.org/10.1021/acs.jpcc.0c03106
J. Phys. Chem. C 2020, 124, 18275−18283

carbon 1s to the dopant-centered LUMO (a″ for the H_4-aggregate and e_x for the NV^- center). It is important to note that both of these systems have very similar energetic values for their pre-edge features. In the case of the H_4 system, the unoccupied orbitals are localized on the top nitrogen and vacancy pair and as such behave similarly to that of the NV^- system. The pre-edge feature in H_4-aggregate and NV^- systems is ∼3 eV red-shifted in comparison to the pure diamond peak. This is less than the ∼5 eV shift which was previously reported in the presence of silicon split-vacancy centers or of surface reorganization in nanodiamonds,[11,12] and as such may be useful for distinguishing between the various systems.

In the case of the nitrogen K-edge, a pure diamond system will not have responses due to the absence of nitrogens in the system. As is reported in Table 3, the nitrogen K-edge of the nitrogen-containing nanodiamonds are in the ∼402 eV range. This energetic range is similar to that for trivalent nitrogen in non-aromatic organic molecules.[69] It can be noted that the B-aggregate is blue-shifted in comparison to the H_4-aggregate and NV^- centers as is also seen for the carbon K-edge responses. It should be noted that the response by the H_4-aggregate and NV^- center are similar since (as can be seen in Figure S17) the leaving orbital for the response is the top nitrogen, which, as referenced earlier, behaves similar to an NV^- center. However, the H_4-aggregate center response is slightly blue-shifted, indicating that the electron density for the center is slightly less than that of the isolated NV^- center. These responses can be beneficial for examining the nature of the nitrogen doping within the nanodiamond and can be experimentally realized through processes such as scanning transmission X-ray absorption microscopy to compare with theoretical predictions. Additionally, to further distinguish between NV^- centers and the B-aggregate, it may be possible to take advantage of polarized XAS as the NV^- centers, due to the non-centrosymmetric one-dimensional C_{3v} rotation axis, will have polarization-dependent spectra while the B-aggregate, due to the centrosymmetric T_d symmetry, will not. This can be seen by examining the electronic transition dipoles for the nitrogen K-edge transitions where in the case of the NV^- center the only strength lies along the ⟨1, 1, 1⟩ axis which the NV^- center is aligned with, while in the case of the B-aggregate there is dipole strength along both the ⟨1, 1, 1⟩ as well as the ⟨1,1,0⟩ axis. One potential issue with this is that the NV center has four potential arrangements; however, work has been done previously to constrain the NV orientation during synthesis.[7]

CONCLUSION

In this work spectroscopic features arising from introducing nitrogen aggregates into a nanodiamond lattice were investigated. It was determined that the presence of nitrogen aggregates introduced features unique from either NV^- systems or pure nanodiamonds into their vibrational spectra. Unfortunately the infrared spectroscopic responses for both aggregate systems were very similar in the ∼800 to ∼1200 cm^{-1} range which sets them apart from either NV^- or pure diamond systems. It was shown that optical absorption spectroscopy can differentiate between the two investigated aggregate systems with the B-aggregate system introducing transitions at ∼4.5 eV and the H_4-aggregate system introducing responses at ∼3.3 eV. It was also shown that these aggregate systems affect the pre-edge region (∼285 eV) of carbon's K-edge XAS. This information can be used to differentiate further between the aggregate systems and possibly other doped diamond species. In this study, though the predicted responses in the XAS can be difficult to detect due to surface defects[12] or other dopant species,[11] chemical treatments of the nanodiamond system can help reveal these features.[2,34,35] In addition we were able to identify vibrational and optical fingerprints of the N_4V_x-aggregate systems aiding in the future detection and characterization of these defect systems.

ASSOCIATED CONTENT

Supporting Information

The Supporting Information is available free of charge at https://pubs.acs.org/doi/10.1021/acs.jpcc.0c03106.

Methodology for formation energy calculations, additional TDDFT calculations, visualizations for the vibrational modes, and visualizations of transitions, as well as information pertaining to the quantum confinement behavior of the aggregate centers (PDF)

AUTHOR INFORMATION

Corresponding Author

Xiaosong Li − *Department of Chemistry, University of Washington, Seattle, Washington 98195, United States;* orcid.org/0000-0001-7341-6240; Email: xsli@uw.edu

Authors

Ryan A. Beck − *Department of Chemistry, University of Washington, Seattle, Washington 98195, United States;* orcid.org/0000-0002-2953-970X

Lixin Lu − *Department of Chemistry, University of Washington, Seattle, Washington 98195, United States*

Alessio Petrone − *Dipartimento di Scienze Chimiche, Università di Napoli Federico II, Complesso Universitario di M. S. Angelo, I-80126 Napoli, Italy;* orcid.org/0000-0003-2232-9934

Amanda C. Ong − *Department of Chemistry, University of Washington, Seattle, Washington 98195, United States*

Peter J. Pauzauskie − *Department of Materials Science, University of Washington, Seattle, Washington 98195, United States; Physical Sciences Division, Pacific Northwest National Laboratory, Richland, Washington 99352, United States;* orcid.org/0000-0002-1554-5949

Complete contact information is available at: https://pubs.acs.org/10.1021/acs.jpcc.0c03106

Notes

The authors declare no competing financial interest.

ACKNOWLEDGMENTS

The development of the computational spectroscopy method is supported by the NSF (Grant CHE-1856210 to X.L.). Study of defects in nanodiamond is supported by the University of Washington Molecular Engineering Materials Center (Grant DMR-1719797) and NSF (Grant NSF-CAREER 1555007 to P.J.P.). A.P. thanks MIUR (Project AIM1829571-1 CUPE61G19000090002) for financial support. This work was facilitated though the use of advanced computational, storage, and networking infrastructure provided by the Hyak supercomputer system and funded by the STF at the University of Washington.

REFERENCES

(1) Bawendi, M. G.; Steigerwald, M. L.; Brus, L. E. The Quantum Mechanics of Larger Semiconductor Clusters ("Quantum Dots"). *Annu. Rev. Phys. Chem.* **1990**, *41*, 477−496.

(2) Holt, K. Diamond at the Nanoscale: Applications of Diamond Nanoparticles from Cellular Biomarkers to Quantum Computing. *Philos. Trans. R. Soc., A* **2007**, *365*, 2845−2861.

(3) Balasubramanian, G.; Chan, I.; Kolesov, R.; Al-Hmoud, M.; Tisler, J.; Shin, C.; Kim, C.; Wojcik, A.; Hemmer, P.; Krueger, A.; et al. Nanoscale Imaging Magnetometry with Diamond Spins Under Ambient Conditions. *Nature* **2008**, *455*, 648−651.

(4) Galli, G. In *Computer-Based Modeling of Novel Carbon Systems and Their Properties: Beyond Nanotubes*; Colombo, L., Fasolino, A., Eds.; Springer: Dordrecht, The Netherlands, 2010; pp 37−56.

(5) Pezzagna, S.; Rogalla, D.; Wildanger, D.; Meijer, J.; Zaitsev, A. Creation and Nature of Optical Centres in Diamond for Single-Photon Emission-Overview and Critical Remarks. *New J. Phys.* **2011**, *13*, 035024.

(6) Mortet, V.; Zhang, L.; Eckert, M.; D'Haen, J.; Soltani, A.; Moreau, M.; Troadec, D.; Neyts, E.; De Jaeger, J.-C.; Verbeeck, J.; et al. Grain Size Tuning of Nanocrystalline Chemical Vapor Deposited Diamond by Continuous Electrical Bias Growth: Experimental and Theoretical Study. *Phys. Status Solidi A* **2012**, *209*, 1675−1682.

(7) Karin, T.; Dunham, S.; Fu, K.-M. Alignment of the Diamond Nitrogen Vacancy Center by Strain Engineering. *Appl. Phys. Lett.* **2014**, *105*, 053106.

(8) Dolde, F.; Doherty, M. W.; Michl, J.; Jakobi, I.; Naydenov, B.; Pezzagna, S.; Meijer, J.; Neumann, P.; Jelezko, F.; Manson, N. B.; et al. Nanoscale Detection of a Single Fundamental Charge in Ambient Conditions Using the NV^- Center in Diamond. *Phys. Rev. Lett.* **2014**, *112*, 097603.

(9) Drake, M.; Scott, E.; Reimer, J. Influence of Magnetic Field Alignment and Defect Concentration on Nitrogen-Vacancy Polarization in Diamond. *New J. Phys.* **2016**, *18*, 013011.

(10) Petrone, A.; Goings, J. J.; Li, X. Quantum Confinement Effects on Optical Transitions in Nanodiamonds Containing Nitrogen Vacancies. *Phys. Rev. B: Condens. Matter Mater. Phys.* **2016**, *94*, 165402.

(11) Petrone, A.; Beck, R. A.; Kasper, J. M.; Li, X.; Huang, Y.; Crane, M.; Pauzauskie, P. Electronic Structures and Spectroscopic Signatures of Silicon-Vacancy Containing Nanodiamonds. *Phys. Rev. B: Condens. Matter Mater. Phys.* **2018**, *98*, 205405.

(12) Beck, R.; Petrone, A.; Kasper, J. M.; Crane, M. J.; Pauzauskie, P. J.; Li, X. Effect of Surface Passivation on Nanodiamond Crystallinity. *J. Phys. Chem. C* **2018**, *122*, 8573−8580.

(13) Crane, M. J.; Petrone, A.; Beck, R. A.; Lim, M. B.; Zhou, X.; Li, X.; Stroud, R. M.; Pauzauskie, P. J. High Pressure, High Temperature Molecular Doping of Nanodiamond. *Sci. Adv.* **2019**, *5*, eaau6073.

(14) Levinshtein, M. E.; Rumyantsev, S. L.; Shur, M. *Handbook Series on Semiconductor Parameters: Si, Ge, C (Diamond), GaAs, GaP, GaSb, InAs, InP, InSb*; World Scientific: Singapore, 1996; DOI: 10.1142/2046-vol1.

(15) Mocatta, D.; Cohen, G.; Schattner, J.; Millo, O.; Rabani, E.; Banin, U. Heavily Doped Semiconductor Nanocrystal Quantum Dots. *Science* **2011**, *332*, 77−81.

(16) Eilers, J.; Groeneveld, E.; de Mello Donegá, C.; Meijerink, A. Optical Properties of Mn-Doped ZnTe Magic Size Nanocrystals. *J. Phys. Chem. Lett.* **2012**, *3*, 1663−1667.

(17) Manson, N.; Harrison, J. Photo-ionization of the nitrogen-vacancy center in diamond. *Diamond Relat. Mater.* **2005**, *14*, 1705−1710.

(18) Bradac, C.; Gaebel, T.; Naidoo, N.; Sellars, M.; Twamley, J.; Brown, L.; Barnard, A.; Plakhotnik, T.; Zvyagin, A.; Rabeau, J. Observation and Control of Blinking Nitrogen-Vacancy Centres in Discrete Nanodiamonds. *Nat. Nanotechnol.* **2010**, *5*, 345−349.

(19) Manson, N. B.; Beha, K.; Batalov, A.; Rogers, L. J.; Doherty, M. W.; Bratschitsch, R.; Leitenstorfer, A. Assignment of the NV 0 575-nm zero-phonon line in diamond to a 2 E-2 A 2 transition. *Phys. Rev. B: Condens. Matter Mater. Phys.* **2013**, *87*, 155209.

(20) Ranjbar, A.; Babamoradi, M.; Heidari Saani, M.; Vesaghi, M. A.; Esfarjani, K.; Kawazoe, Y. Many-Electron States of Nitrogen-Vacancy Centers in Diamond and Spin Density Calculations. *Phys. Rev. B: Condens. Matter Mater. Phys.* **2011**, *84*, 165212.

(21) Doherty, M. W.; Manson, N. B.; Delaney, P.; Jelezko, F.; Wrachtrup, J.; Hollenberg, L. C. L. The Nitrogen-Vacancy Colour Centre in Diamond. *Phys. Rep.* **2013**, *528*, 1−45.

(22) Deák, P.; Aradi, B.; Kaviani, M.; Frauenheim, T.; Gali, A. Formation of NV Centers in Diamond: A Theoretical Study Based on Calculated Transitions and Migration of Nitrogen and Vacancy Related Defects. *Phys. Rev. B: Condens. Matter Mater. Phys.* **2014**, *89*, 075203.

(23) Gali, A. *Ab initio* Theory of the Nitrogen-Vacancy Center in Diamond. *Nanophotonics* **2019**, *8*, 1907−1943.

(24) Jones, R.; Briddon, P. R.; Öberg, S. First-principles Theory of Nitrogen Aggregates in Diamond. *Philos. Mag. Lett.* **1992**, *66*, 67−74.

(25) Davies, G. Dynamic Jahn-Teller distortions at trigonal optical centres in diamond. *J. Phys. C: Solid State Phys.* **1979**, *12*, 2551−2566.

(26) Rakhmanova, M. I.; Nadolinny, V. A.; Yuryeva, O. P.; Pokhilenko, N. P.; Logvinova, A. M. Peculiarities of Nitrogen Impurity Aggregation in Diamonds from the Sytykanskaya Pipe, Yakutia. *Eur. J. Mineral.* **2015**, *27*, 51−56.

(27) Jones, R.; Torres, V.; Briddon, P.; Öberg, S. Theory of Nitrogen Aggregates in Diamond: The H3 and H4 Defects. *Mater. Sci. Forum* **1993**, *143−147*, 45−50.

(28) Salustro, S.; Ferrari, A. M.; gentile, F. S.; Desmarais, J. K.; Rerat, M.; Dovesi, R. Characterization of the B-Center Defect in Diamond Through the Vibrational Spectrum: A Quantum-Mechanical Approach. *J. Phys. Chem. A* **2018**, *122*, 594−600.

(29) Mainwood, A. Nitrogen and Nitrogen-Vacancy Complexes and their Formation in Diamond. *Phys. Rev. B: Condens. Matter Mater. Phys.* **1994**, *49*, 7934−7941.

(30) Pople, J. A.; Beveridge, D. L. *Approximate Molecular Orbital Theory*; McGraw-Hill: New York, NY, USA, 1970.

(31) Sun, S.; Beck, R. A.; Williams-Young, D. B.; Li, X. Simulating Magnetic Circular Dichroism Spectra with Real-Time Time-Dependent Density Functional Theory in Gauge Including Atomic Orbitals. *J. Chem. Theory Comput.* **2019**, *15*, 6824−6831.

(32) Goings, J. J.; Schimpf, A. M.; May, J. W.; Johns, R. W.; Gamelin, D. R.; Li, X. Theoretical Characterization of Conduction-Band Electrons in Photodoped and Aluminum-Doped Zinc Oxide (AZO) Quantum Dots. *J. Phys. Chem. C* **2014**, *118*, 26584−26590.

(33) Leger, J. D.; Friedfeld, M. R.; Beck, R. A.; Gaynor, J. D.; Petrone, A.; Li, X.; Cossairt, B. M.; Khalil, M. Carboxylate Anchors Act as Exciton Reporters in 1.3 nm Indium Phosphide Nanoclusters. *J. Phys. Chem. Lett.* **2019**, *10*, 1833−1839.

(34) Arnault, J.-C.; Petit, T.; Girard, H.; Chavanne, A.; Gesset, C.; Sennour, M.; Chaigneau, M. Surface Chemical Modifications and Surface Reactivity of Nanodiamonds Hydrogenated by CVD Plasma. *Phys. Chem. Chem. Phys.* **2011**, *13*, 11481−11487.

(35) John, P.; Stoikou, M. D. Hydrogen Plasma Interaction with (100) Diamond Surfaces. *Phys. Chem. Chem. Phys.* **2011**, *13*, 11503−11510.

(36) Pauzauskie, P. J.; Crowhurst, J. C.; Worsley, M. A.; Laurence, T. A.; Kilcoyne, A. L. D.; Wang, Y.; Willey, T. M.; Visbeck, K. S.; Fakra, S. C.; Evans, W. J.; et al. Synthesis and Characterization of a Nanocrystalline Diamond Aerogel. *Proc. Natl. Acad. Sci. U. S. A.* **2011**, *108*, 8550−8553.

(37) Mochalin, V. N.; Shenderova, O.; Ho, D.; Gogotsi, Y. The Properties and Applications of Nanodiamonds. *Nat. Nanotechnol.* **2012**, *7*, 11−23.

(38) Takahashi, K.; Yoshikawa, A.; Sandhu, A. *Wide Bandgap Semiconductors: Fundamental Properties and Modern Photonic and Electronic Devices*; Springer: New York, NY, USA, 2007.

(39) Frisch, M. J.; Trucks, G. W.; Schlegel, H. B.; Scuseria, G. E.; Robb, M. A.; Cheeseman, J. R.; Scalmani, G.; Barone, V.; Petersson,

https://dx.doi.org/10.1021/acs.jpcc.0c03106
J. Phys. Chem. C 2020, 124, 18275−18283

G. A.; Nakatsuji, H.; et al. *Gaussian 16*, Rev. B.01; Gaussian: Wallingford, CT, USA, 2016.
(40) Becke, A. D. Density-Functional Thermochemistry. III. The Role of Exact Exchange. *J. Chem. Phys.* **1993**, *98*, 5648.
(41) Lee, C.; Yang, W.; Parr, R. G. Development of the Colle-Salvetti Correlation-Energy Formula into a Functional of the Electron Density. *Phys. Rev. B: Condens. Matter Mater. Phys.* **1988**, *37*, 785.
(42) Miehlich, B.; Savin, A.; Stoll, H.; Preuss, H. Results Obtained with the Correlation Energy Density Functionals of Becke and Lee, Yang and Parr. *Chem. Phys. Lett.* **1989**, *157*, 200−206.
(43) Yanai, T.; Tew, D. P.; Handy, N. C. A New Hybrid Exchange-Correlation Functional Using the Coulomb-Attenuating Method (CAM-B3LYP). *Chem. Phys. Lett.* **2004**, *393*, 51−57.
(44) Vörös, M.; Gali, A. Optical Absorption of Diamond Nanocrystals from Ab Initio Density-Functional Calculations. *Phys. Rev. B: Condens. Matter Mater. Phys.* **2009**, *80*, 161411.
(45) Kaviani, M.; Deák, P.; Aradi, B.; Frauenheim, T.; Chou, J.-P.; Gali, A. Proper Surface Termination for Luminescent Near-Surface NV Centers in Diamond. *Nano Lett.* **2014**, *14*, 4772−4777.
(46) Vlasov, I. I.; Shiryaev, A. A.; Rendler, T.; Steinert, S.; Lee, S.-Y.; Antonov, D.; Vörös, M.; Jelezko, F.; Fisenko, A. V.; Semjonova, L. F.; et al. Molecular-Sized Fluorescent Nanodiamonds. *Nat. Nanotechnol.* **2014**, *9*, 54−58.
(47) Lin, C.-K.; Wang, Y.-H.; Chang, H.-C.; Hayashi, M.; Lin, S. H. One-and Two-Photon Absorption Properties of Diamond Nitrogen-Vacancy Defect Centers: A Theoretical Study. *J. Chem. Phys.* **2008**, *129*, 124714.
(48) Gali, A. Time-Dependent Density Functional Study on the Excitation Spectrum of Point Defects in Semiconductors. *Phys. Status Solidi B* **2011**, *248*, 1337−1346.
(49) Casida, M. E. In *Recent Advances in Density Functional Methods*, Part I; Chong, D. P., Ed.; World Scientific Publishing: Singapore, 1995; Vol. *1*; pp 155−193, DOI: 10.1142/9789812830586_0005.
(50) Dreuw, A.; Head-Gordon, M. Single-reference ab initio methods for the calculation of excited states of large molecules. *Chem. Rev.* **2005**, *105*, 4009−4037.
(51) Stratmann, R. E.; Scuseria, G. E.; Frisch, M. J. An Efficient Implementation of Time-Dependent Density-Functional Theory for the Calculation of Excitation Energies of Large Molecules. *J. Chem. Phys.* **1998**, *109*, 8218−8224.
(52) Dreuw, A.; Head-Gordon, M. Single-Reference Ab Initio Methods for the Calculation of Excited States of Large Molecules. *Chem. Rev.* **2005**, *105*, 4009−4037.
(53) Liang, W.; Fischer, S. A.; Frisch, M. J.; Li, X. Energy-Specific Linear Response TDHF/TDDFT for Calculating High-Energy Excited States. *J. Chem. Theory Comput.* **2011**, *7*, 3540−3547.
(54) Lestrange, P. J.; Nguyen, P. D.; Li, X. Calibration of Energy-Specific TDDFT for Modeling K-Edge XAS Spectra of Light Elements. *J. Chem. Theory Comput.* **2015**, *11*, 2994−2999.
(55) Vins, V.; Eliseev, A. Effect of Annealing at High Pressures and Temperatues on the Defect-Admixture Structure of Natural Diamonds. *Inorg. Mater. Appl. Research* **2010**, *1*, 303−310.
(56) Ando, T.; Ishii, M.; Kamo, M.; Sato, Y. Diffuse Reflectance Infrared Fourier-Transform Study of the Plasma Hydrogenation of Diamond Surfaces. *J. Chem. Soc., Faraday Trans.* **1993**, *89*, 1383−1386.
(57) Stehlik, S.; Varga, M.; Ledinsky, M.; Jirasek, V.; Artemenko, A.; Kozak, H.; Ondic, L.; Skakalova, V.; Argentero, G.; Pennycook, T.; et al. Size and Purity Control of HPHT Nanodiamonds dDown to 1 nm. *J. Phys. Chem. C* **2015**, *119*, 27708−27720.
(58) Negri, F.; Castiglioni, C.; Tommasini, M.; Zerbi, G. A Computational Study of the Raman Spectra of Large Polycyclic Aromatic Hydrocarbons: Toward Molecularly Defined Subunits of Graphite. *J. Phys. Chem. A* **2002**, *106*, 3306−3317.
(59) Filik, J.; Harvey, J. N.; Allan, N. L.; May, P. W.; Dahl, J. E. P.; Liu, S.; Carlson, R. M. K. Raman Spectroscopy of Nanocrystalline Diamond: An ab initio Approach. *Phys. Rev. B: Condens. Matter Mater. Phys.* **2006**, *74*, 035423.
(60) Hachtel, J. A.; Huang, J.; Popovs, I.; Jansone-Popova, S.; Keum, J. K.; Jakowski, J.; Lovejoy, T. C.; Dellby, N.; Krivanek, O. L.; Idrobo, J. C. Identification of Site-Specific Isotopic Labels by Vibrational Spectroscopy in the Electron Microscope. *Science* **2019**, *363*, 525−528.
(61) Li, Z.; Aleshire, K.; Kuno, M.; Hartland, G. V. Super-Resolution Far-Field Infrared Imaging by Photothermal Heterodyne Imaging. *J. Phys. Chem. B* **2017**, *121*, 8838−8846.
(62) Martin, R. L. Natural Transition Orbitals. *J. Chem. Phys.* **2003**, *118*, 4775−4777.
(63) Moseley, H. XCIII. The High-Frequency Spectra of the Elements. *London, Edinburgh, and Dublin Philosophical Magazine and Journal of Science* **1913**, *26*, 1024−1034.
(64) Moseley, H. The High-Frequency Spectra of the Elements. Part II. *London, Edinburgh, and Dublin Philosophical Magazine and Journal of Science* **1914**, *27*, 703−713.
(65) Stöhr, J. *NEXAFS Spectroscopy*; Springer-Verlag: Berlin, Heidelberg, Germany, 1992.
(66) Nilsson, A.; Pettersson, L. G. M. Chemical Bonding on Surfaces Probed by X-Ray Emission Spectroscopy and Density Functional Theory. *Surf. Sci. Rep.* **2004**, *55*, 49−167.
(67) Raty, J.-Y.; Galli, G.; Bostedt, C.; van Buuren, T. W.; Terminello, L. J. Quantum Confinement and Fullerenelike Surface Reconstructions in Nanodiamonds. *Phys. Rev. Lett.* **2003**, *90*, 037401.
(68) Castrucci, P.; Scarselli, M.; De Crescenzi, M.; El Khakani, M. A.; Rosei, F. Probing the Electronic Structure of Carbon Nanotubes by Nanoscale Spectroscopy. *Nanoscale* **2010**, *2*, 1611−1625.
(69) Vairavamurthy, A.; Wang, S. Organic Nitrogen in Geo-macromolecules: Insights on Speciation and Transformation with K-edge XANES Spectroscopy. *Environ. Sci. Technol.* **2002**, *36*, 3050−3056.

https://dx.doi.org/10.1021/acs.jpcc.0c03106
J. Phys. Chem. C 2020, 124, 18275−18283